ACS SENSORS

pubs.acs.org/acssensors Article

2D Conductive Covalent Organic Frameworks with Abundant Carbonyl Groups for Electrochemical Sensing

Kai Niu, Yuying Zhang, Jiping Chen, and Xianbo Lu*

Cite This: https://doi.org/10.1021/acssensors.2c02014 Read Online

ACCESS | Metrics & More | Article Recommendations | Supporting Information

ABSTRACT: Due to their permanent porosity, robust chemical stability, and tunable structure, covalent organic frameworks (COFs) are very attractive in the application of energy storage, catalysis, sorption, and sensing. However, the very low conductivity of COFs severely restricts their application in electrochemical sensing. Here, an aza-fused π-conjugated COFs with abundant carbonyl groups (COF1) was synthesized and deployed as electrode materials in electrochemical sensing for the first time. The current response of the acetylcholinesterase biosensor based on COF1 increases three times when compared to the electrode without COF1. The effects of carbonyl groups on signal enhancement were proved in depth by a series of characterization and comparison experiments with the prepared COF2 without carbonyl groups. The results demonstrated that exposed carbonyl active sites of COF1 can promote the effective immobilization and bioactivity preserving of enzyme molecules and contribute to the enrichment of analytes. Together with the good conductivity of COF1 derived from a fully extended 2D aromatized π-conjugated system, all of which improve the biosensor performance. The COF1-based biosensor exhibited fast response speed, high sensitivity, good selectivity and practicability, and robust stability for organophosphorus pesticide detection and proved to be a promising tool for the rapid and onsite detection of organophosphorus pesticides in the environment.

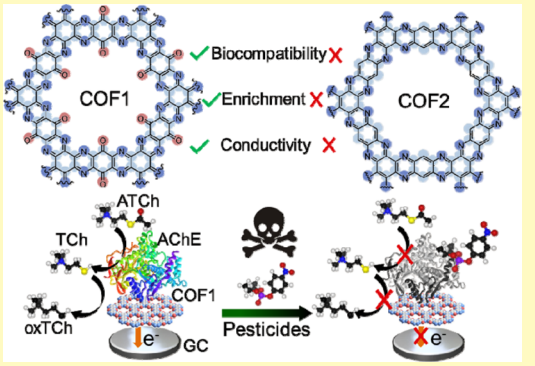

KEYWORDS: *acetylcholinesterase, biosensor, COFs, enrichment effect, organophosphorus pesticides*

Covalent organic frameworks (COFs), an emerging type of highly porous crystalline polymers with periodic structures, are purely organic materials connected by strong covalent bonds among the organic structural units.[1,2] COFs possess the characteristics of permanent porosity, high surface area, robust chemical stability, and good biocompatibility. More significantly, the backbone structure of COFs can be designed at the atomic level. Therefore, these advantages have facilitated the COFs as promising materials for a wide range of applications, including energy storage,[3,4] gas sorption and separation,[5,6] optoelectronics,[7,8] catalysis,[9,10] drug delivery,[11,12] sensing,[13,14] and so forth.

Electrochemical sensing is based on the measurable electrical signal change produced by the interaction between analyte molecules and electrodes. Electrochemical sensors have been extensively studied for clinical diagnostics, biochemistry, and environmental monitoring because they provide several advantages over other analytical methods, such as fast response, high efficiency, cost-effective, and simplicity of operation.[15−18] The advantageous characteristics of COFs can lead to accumulation and rapid mass transfer of analyte molecules, further amplifying the signal response and thus increasing sensitivity, locating COFs as superior candidate materials for electrochemical sensing. Unfortunately, COFs have mostly been employed as fluorescent sensors[19,20] and scaffolds in biosensors[21,22] rather than electrode modifying materials due to very low conductivity. Therefore, from the perspective of electrochemical sensing, exploring COFs with good conductivity is essentially required.[23]

Recently, there is a narrow class of 2D aza-fused π-conjugated COFs that has exhibited favorable conductivity among the reported COFs.[24−26] The completely extended 2D aromatized π-conjugated system in these COFs, along with the long-range $\pi-\pi$ stacking, offers an uninterrupted channel for the electrons, allowing the resulting material to conduct electricity. Indeed, the fascinating capabilities of these COFs, namely the conductive network related to an easily functionalized pore structure, provide possibilities for their investigation in electrochemical sensing applications. Yet, to the best of our understanding, no detailed research employing aza-fused pure COFs as electrode materials for electrochemical sensing has been reported.

Organophosphorus pesticides have been extensively used in the agriculture business all over the world to eradicate insects

Received: September 14, 2022
Accepted: October 12, 2022

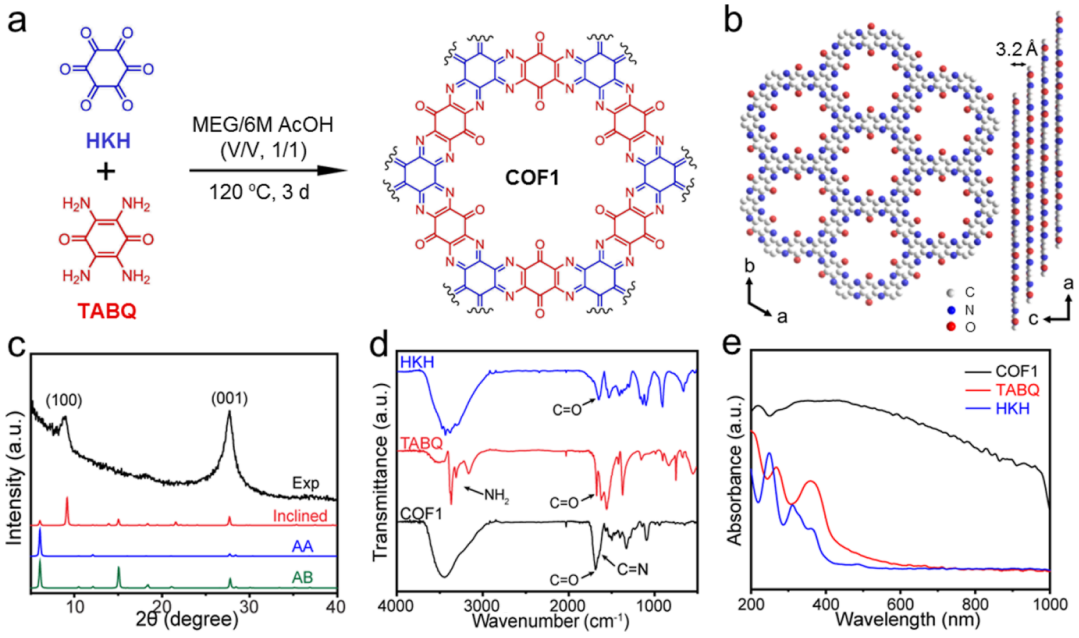

Figure 1. Structure and characterization of COF1. (a) Synthesis route of COF1. (b) Top- and side-view of the inclined stacking model of COF1. (c) Experimental and simulated XRD patterns of COF1. (d) FTIR spectra and (e) UV/Vis spectra of HKH, TABQ, and COF1.

and boost crop output. The excessive use of organophosphorus pesticides in agriculture, on the other hand, invariably results in pesticide residues in soil, water, and food, posing a major hazard to the environment and human health. These pesticides, even when exposed in vivo in a small amount, can quickly bind irreversibly to the active site of acetylcholinesterase (AChE) and subsequently disrupt the metabolism of neurotransmitters, which could result in the dysfunction of the nervous system, respiratory failure, and even death.[27,28] Hence, there is an urgent need to develop a rapid, onsite, and reliable analysis method for the detection of organophosphorus pesticides.

Herein, we synthesized a kind of 2D conductive COFs with abundant carbonyl groups (COF1) via a simple hydrothermal method. The distinctive structure and superior properties of COF1 make it an ideal electrode material for enzyme-based biosensors. As a demonstration, AChE was chosen as a model enzyme to prepare an electrochemical biosensor in which COF1 was used as electrode material. Interestingly, the resulting biosensor showed a significantly enhanced electrochemical response compared to the biosensor without COF1. To better study the structure−property relationship in COF1, we prepared COF2 without carbonyl groups for comparison. Through a series of characterization and comparative experiments in terms of biocompatibility, enrichment effect, conductivity, and surface area, the key role of carbonyl groups in signal enhancement was proved. Inspired by the attractive performance of the biosensor, we next used it to detect paraoxon, an organophosphorus pesticide that is highly toxic and widely used in agriculture. Under the optimized experimental conditions, the biosensor demonstrated fast response speed, high sensitivity, good selectivity, robust stability, and good recovery rate for paraoxon in real samples, which showed a promising method for the rapid and onsite detection of organophosphorus pesticides in the environment.

EXPERIMENTAL SECTION

Chemicals and Materials. AChE from electrophorus electricus, acetylthiocholine chlorine (ATCh), and nafion were purchased from Sigma-Aldrich (Shanghai, China). 2,3,5,6-Tetraaminobenzoquinone CAS: 1128-13-8 (TABQ) and 5,5′-dithiobis-(2-nitrobenzoic acid) (DTNB) were purchased from Shanghai Haohong Scientific Co., Ltd (Shanghai, China). Hexaketocyclohexane octahydrate CAS: 527-31-1 (HKH), 1,2,4,5-tetraaminobenzene tetrahydrochloride CAS: 4506-66-5 (TAB), ethylene glycol (MEG), acetic acid (AcOH), anhydrous DMF, glucose, and urea were purchased from Aladdin Biochemical Technology Co., Ltd (Shanghai, China). Paraoxon was purchased from Tan-Mo Technology Co., Ltd (Beijing, China). Deionized water (18 MΩ cm), obtained from a Milli-Q purification system (Millipore, MA, USA), was used in all experiments. Phosphate buffer solution (PBS, 50 mM, pH 7.0) was used in electrochemical measurements.

Synthesis of COF1. TABQ (0.14 mmol, 23.5 mg) and HKH (0.09 mmol, 28.1 mg) were added in the mixed solution of MEG (10 mL) and AcOH (6 M, 10 mL) in a screw-capped Pyrex tube under a nitrogen atmosphere. After sonication for 15 min, the tube was transferred to a preheated oven at 65 °C for 1 day followed by 120 °C heating for 3 days. The obtained COF1 powders were isolated by centrifugation (8000 rpm, 5 min) and washed with deionized water, acetone, and tetrahydrofuran several times and dried at 80 °C under vacuum for 1 day.

Synthesis of COF2. TAB (1.875 mmol, 532.5 mg) was dissolved in 15 mL of anhydrous DMF, and HKH (1.25 mmol, 390 mg) was dissolved in 5 mL of anhydrous DMF. Two solutions were mixed and refluxed for 2 days under a nitrogen atmosphere. The obtained COF2 powders were isolated by centrifugation (8000 rpm, 5 min) and washed with deionized water, acetone, and tetrahydrofuran several times and dried at 80 °C under vacuum for 1 day.

Preparation of Biosensors. All glassy carbon (GC) electrodes were polished using 1, 0.3, and 0.05 μm alumina slurry on a polishing pad, followed by sonication in deionized water and ethanol to give the electrodes a mirror finish. The biosensor was prepared layer-by-layer by drop-casting 4 μL of COF solution (0.2 mg mL^{-1}, dissolved in deionized water), 4 μL of AChE solution (0.1 U μL^{-1}, dissolved in 50 mM PBS, pH 7.0), and 4 μL of nafion solution (0.5%, dissolved in deionized water) on a freshly polished GC electrode. After each step, the electrode was dried at room temperature, and the biosensor was

https://doi.org/10.1021/acssensors.2c02014
ACS Sens. XXXX, XXX, XXX−XXX

bathed in PBS for 15 min prior to electrochemical experiments. The biosensor was kept in a refrigerator at 4 °C while not in use.

Detection of Paraoxon. Paraoxon was detected using cyclic voltammetry (CV) in the potential range of 0.3−1.0 V. The biosensor was immersed in a solution containing varying amounts of paraoxon for 15 min. Then, the biosensor was transferred into 1 mM ATCh solution for CV measurements. The inhibition rate (I %) of paraoxon was calculated as follows $I\ \% = (I_0 - I_1)/I_0 \times 100\%$, where I_0 and I_1 stand for the current values before and after the exposure of paraoxon, respectively.

RESULTS AND DISCUSSION

Characterization of COF1. As depicted in Figure 1a, we synthesized COF1 by a hydrothermal method using HKH and TABQ at 120 °C. The powder X-ray diffraction (PXRD) pattern was used to analyze the crystalline architecture of bulky powder of COF1 (Figure 1c). There are two broad peaks visible at nearly $2\theta = 8.9$ and 27.8°, which could be assigned to (100) and (001) planes. Due to the $\pi-\pi$ stacking between the adjacent layers, COF1 exhibited a typical layer structure with a small layer spacing of 3.2 Å. However, COF1 was not an ideal eclipsed stacking model because of the steric hindrance and the charge repulsion from polar heteroatoms (nitrogen and oxygen). By comparing different simulated stacking models, we determined that the experimental XRD data match the inclined stacking model better (Figure 1b,c).[29,30]

The as-prepared COF1 was further investigated using Fourier transform infrared (FTIR) spectroscopy, ^{13}C solid-state nuclear magnetic resonance (13C NMR) spectroscopy, and UV/Vis spectra, in which the complete conversion of reactive groups and formation of linkage were confirmed. The active reaction groups of HKH and TABQ, carbonyl and amino group, were probed in FTIR spectra (Figure 1d) by the appearance of the C═O stretching vibration (1644 cm^{-1}) and the N−H stretching vibration (3300−3500 cm^{-1}), respectively. After the carbonyl and amino groups of monomers disappear during polymerization, COF1 exhibited a new absorption peak at 1626 cm^{-1} for the characteristic vibration of the C═N bond, indicating the presence of imine linkages. Besides, the inert reactive carbonyl groups of TABQ were retained in COF1 causing the band at 1682 cm^{-1}. The solid-state ^{13}C NMR spectrum of COF1 showed the chemical shifts at around 149 and 172 ppm (Figure S1), demonstrating the formation of imine linkages and the retention of carbonyl groups. The abundant carbonyl of COF1, which in principle can form hydrogen bonds with the amino and carboxyl groups in the enzyme molecules, could offer a favorable biocompatible microenvironment for the enzyme, thereby sustaining its catalytic activity and stability. Moreover, the UV/Vis spectra of COF1 show a broad band from 400 to 1000 nm compared with HKH and TABQ (Figure 1e), which confirmed that the π-electron of COF1 cloud delocalize.[31,32] The highly ordered conjugation systems enable COF1 to have the ability to conduct electricity.

The microstructure of COF1 was examined by scanning electron microscopy (SEM) and high-resolution transmission electron microscopy (HRTEM). Figure 2a shows a typical SEM image and TEM image (inset) of COF1, in which it is agglomerated as nanorods. The stacking multiple layers of COF1 were evident in the HRTEM image of Figure 2b. The Raman spectrum of COF1 in Figure S2 shows a G band at 1522 cm^{-1}, which represents the sp^2 type carbon atoms in the 2D honeycomb structure, further confirming the graphene-like 2D structure of COF1.[33] Furthermore, the elemental mapping

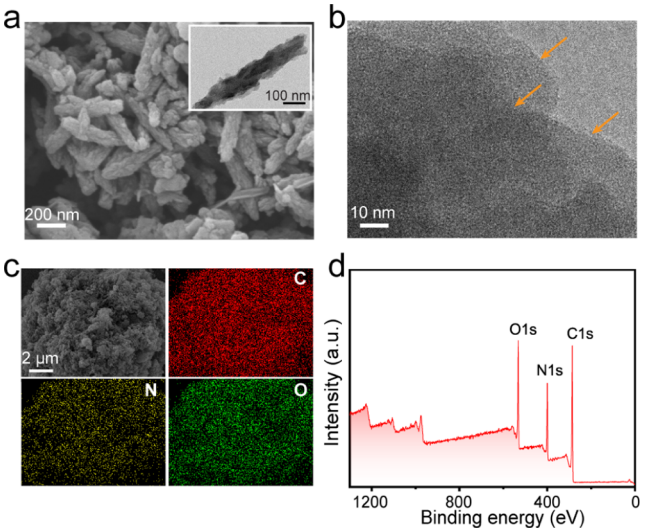

Figure 2. Characterization of COF1. (a) SEM image of COF1, inset: TEM image of COF1. (b) HRTEM image of COF1. (c) Elemental mapping images of COF1. (d) XPS survey spectrum of COF1.

from SEM images validated the uniform spatial distributions of C, N, and O across COF1 (Figure 2c). The chemical composition of COF1 is further exhibited in the wide-scan X-ray photoelectron spectroscopy (XPS) spectra in Figure 2d. The high-resolution C 1s spectra confirmed the presence of the $\pi-\pi^*$ satellite peak, which is due to the strongly interlayer stacking in COF1 (Figure S3a). The abundant C=O and anticipated C=N functionalities were also confirmed from the high-resolution C 1 s and N 1 s, respectively (Figure S3b,c).

Electrochemical Performance of the Biosensor. To evaluate the charge-transfer performance of the modified electrodes, CV and electrochemical impedance spectroscopy (EIS) experiments were performed applying the commonly used $[Fe(CN)_6]^{4-/3-}$ redox probe. Figure 3a demonstrates that by modifying COF1, the effective surface area and response peak current of bare GC can be significantly increased. Interestingly, the peak-to-peak separation of GC/COF1 decreased when compared to bare GC. Such a decrease in peak separation suggested that the reaction kinetics have improved, indicating quicker charge transfer.[34] AChE was effectively immobilized on the surface of GC/COF1, resulting in a lower peak current (the red line, as shown in Figure 3a). This result was due to the dielectric nature of enzyme, which prevents electron transfer on the surface of electrodes. The EIS curves in Figure 3b show a typical semicircle and straight line in the high- and low-frequency scope. The lower electronic-transfer resistance of the GC/COF1 electrode implied more favorable kinetics and better conductivity compared to bare GC. The electronic-transfer resistance of the biosensor increased significantly after the modification of AChE, demonstrating the successful modification of AChE. These findings were in agreement with the findings of the CV measurement.

To begin with, the GC/COF1/AChE electrode was explored as an electrochemical biosensor for the detection of ATCh, which is a derivative of acetylcholine. As shown in Figure 3c, no redox peaks were observed in the absence of ATCh. In the presence of 1 mM ATCh, the GC/COF1/AChE electrode demonstrated an oxidation peak at 0.75 V with a current density of 176 $\mu A\ cm^{-2}$. This could correlate to the

https://doi.org/10.1021/acssensors.2c02014
ACS Sens. XXXX, XXX, XXX−XXX

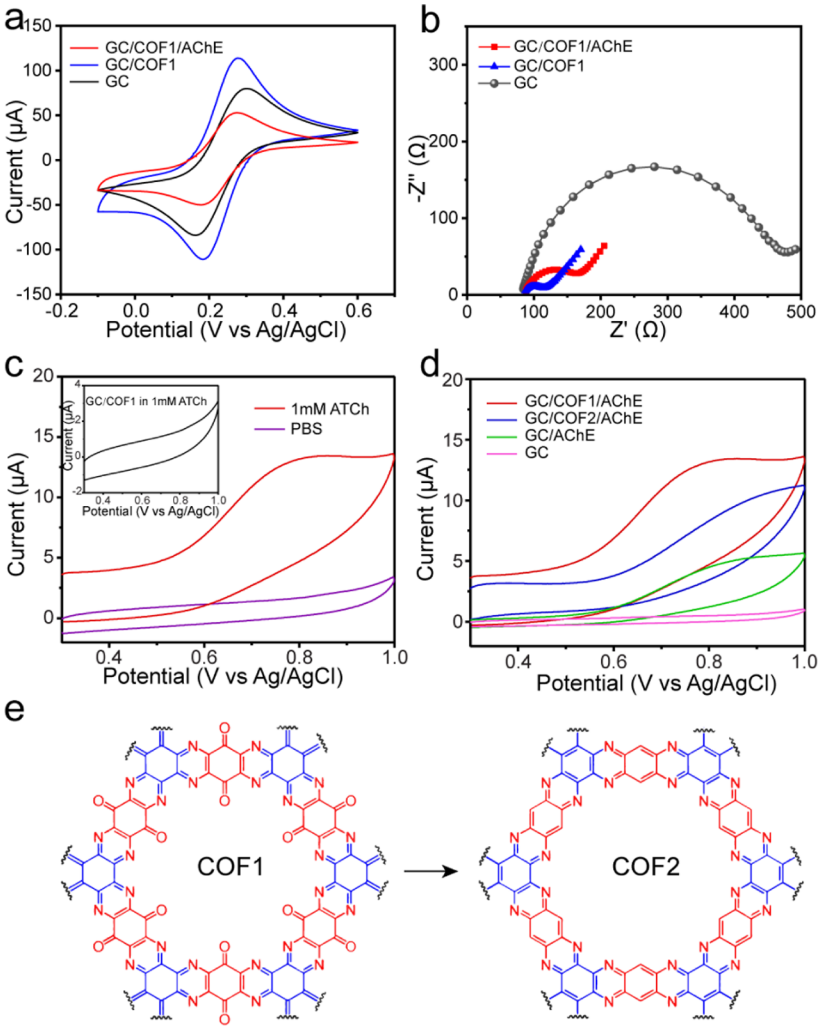

Figure 3. Electrochemical performance of the biosensor. (a) CV and (b) EIS of each modified layer of the proposed biosensor in 0.1 M KCl solution containing 5.0 mM $K_3Fe(CN)_6/K_4Fe(CN)_6$ (1:1). Scan rate: 50 mV s^{-1}. (c) CV profiles of the GC/COF1/AChE electrode in PBS solution in the presence or absence of 1 mM ATCh. Scan rate: 100 mV s^{-1}. Inset: a CV curve of GC/COF1 in 1 mM ATCh. (d) CV curves recorded on different electrodes targeting the oxidation of 1 mM ATCh. Scan rate: 100 mV s^{-1}. (e) Molecular structures of COF1 and COF2.

direct oxidation of thiocholine (TCh), which is an electroactive product of ATCh hydrolyzed by AChE. Moreover, the GC/COF1 electrode showed no peaks in the presence of ATCh (inset of Figure 3c), indicating the importance of enzyme.

To further assess the functions of each biosensor layer and to reasonably compare, (a) bare GC, (b) GC/AChE, and (c) GC/COF2/AChE electrodes were constructed individually. As shown in Figure 3d, the bare GC electrode exhibited no current response for ATCh when compared to that of GC/AChE electrodes, clearly revealing the lack of the catalytic activity of enzyme. Interestingly, the GC/COF1/AChE electrode outperformed the other modified electrodes in terms of the electrochemical performance. The oxidation current on GC/COF1/AChE electrodes increased three times when compared to the GC/AChE electrode. To better study the structure−property relationship in COF1, COF2 was also prepared for comparison, through the polycondensation of TAB and HKH (Figure S4). The different molecular structures of COF1 and COF2 are shown in Figure 3e, in which COF2 lacks carbonyl when compared to COF1. The FTIR spectroscopy monitored the polycondensation of the monomers (Figure S5), and the XRD patterns of COF2 matched well with the reports (Figure S6),[24] indicating the successful preparation of COF2. The superiority of COF1 with abundant carbonyl was proved by the comparative evaluation of GC/COF1/AChE and GC/COF2/AChE electrodes (Figure 3d). The difference in the performance of the COF1 and COF2 based biosensors should not be attributed to carbonyl groups alone but should also be fully considered in terms of conductivity, specific surface area, and so forth, which will be characterized and explored in depth below.

Mechanism of Signal Enhancement. A series of experiments and characterization were further used to focus on the structure−property relationship in COF1. We first chose the centrifugal sedimentation method to prove the interaction between COF and enzyme. As shown in Figure 4a, if COF can adsorb AChE from the mixed solution of COF and AChE, the COF/AChE complex can be easily separated in the function of centrifugal force. Then, the enzyme activity of the COF/AChE complex was evaluated through the following color reaction. The procedure was based on the reaction of the enzymatic product TCh with DTNB, which produces a yellow product of 2-nitro-5-thiobenzoic acid (TNB), as shown in

https://doi.org/10.1021/acssensors.2c02014
ACS Sens. XXXX, XXX, XXX−XXX

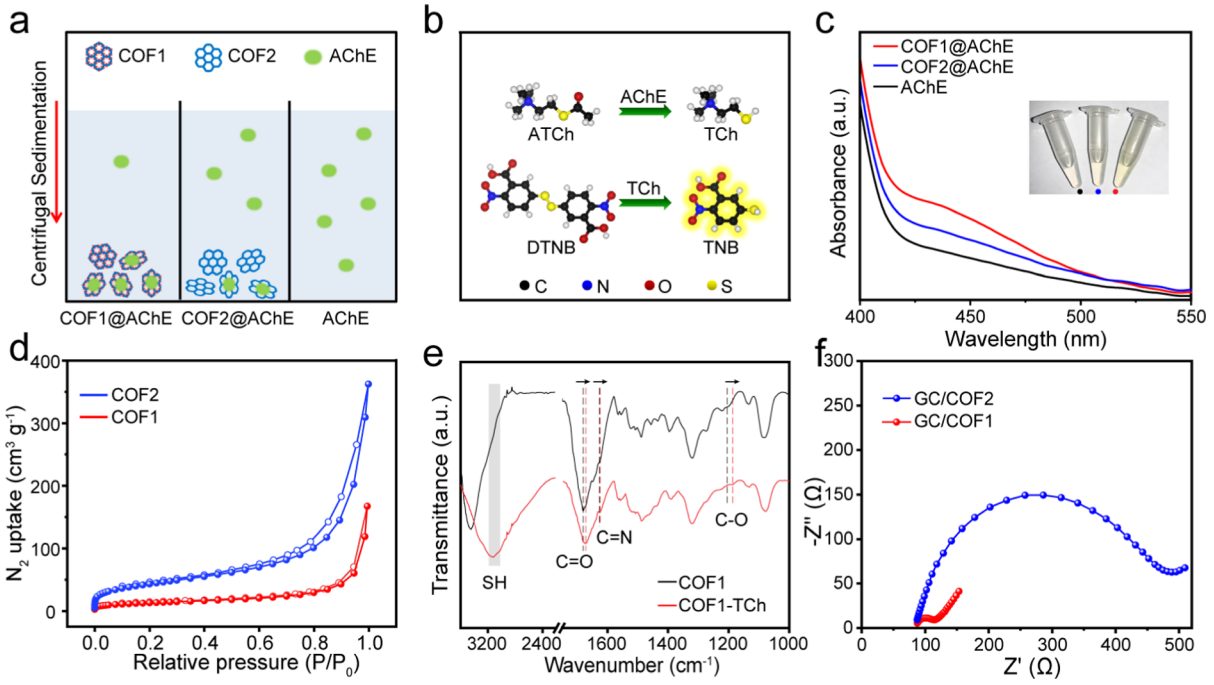

Figure 4. Mechanism of signal enhancement. (a) Principle of centrifugal sedimentation of different samples. (b) Color reaction scheme for the detection of the enzyme activity. (c) UV/Vis spectra of different samples for the color reaction. Inset: photograph showing AChE activities of different samples. (d) N_2 adsorption (solid) and desorption (hollow) curves of COF1 and COF2. (e) FTIR spectra of COF1 and COF1-TCh. (f) EIS of COF1 and COF2 in 0.1 M KCl solution containing 5.0 mM $K_3Fe(CN)_6/K_4Fe(CN)_6$ (1:1).

Figure 4b. After the incubation of the COF/AChE complex in 5 mM ATCh, the clear supernatant contained TCh was separated. The inset of Figure 4c shows that the supernatant of the COF1/AChE sample turned DTNB into a deeper yellow product compared to the other samples. The maximum absorption in the UV/Vis spectra further exhibited superior enzyme activity of the COF1/AChE complex among the as-prepared samples (Figure 4c), proving their ability to accommodate more AChE. However, as shown in Figure 4d, the Brunauer–Emmett–Teller (BET) surface area S_{BET} of COF1 (47 m^2 g^{-1}) was smaller than that of COF2 (154 m^2 g^{-1}). These results revealed that the S_{BET} value and adsorption capacity of the materials were not positively correlated. Indeed, the exposed carbonyl active sites of COF1 can promote the interaction (hydrogen bonds) with the enzyme molecule and effective immobilization of enzyme, leading to enhanced biocompatibility and enzymatic activity, further generating a stronger current signal.

We applied FTIR spectra to study the interactions between COF and TCh, which is the electroactive substance of the electrode reaction. Figure 4e shows typical peaks for SH at 3120 cm^{-1} and a red-shift of C═O, C═N, and C−O of COF1.[35] In the absence of carbonyl, there was only a weak shift of C═N for COF2 (Figure S7). These phenomena pointed to strong interactions between TCh and COF1, which could contribute to the enrichment of TCh, culminating in the superior electrochemical response of GC/COF1/AChE. Besides, we explored the reaction process by the change of current response at different scan rates. Figure S8 shows CVs for the GC/COF1/AChE electrode at different scan rates in 1 mM ATCh. The oxidation potentials shifted to a more positive position with the increasing scan rates, owing to the increased internal diffusion resistance within the biosensor. At the same time, the peak currents rose linearly with the scan rate, indicating that the electrode reaction is a surface-controlled process (inset of Figure S8). These results indicate that the enrichment of TCh on the COF1-based electrode surface plays a key role in improving the electrochemical response of biosensors.

Conductivity should also be considered in the mechanism of signal enhancement. As shown in Figure 4f, when compared to GC/COF1, the smaller electronic-transfer resistance of the GC/COF1 electrode predicted superior conductivity. This phenomenon may be described to the larger conjugate systems of COF1 originating from the abundant carbonyl groups. According to the Randles–Sevcik equation,[36] the effective surface area of GC/COF1 was higher than that of GC/COF2 (Figure S9), which should also be considered in the signal enhancement. Therefore, the mechanism of signal enhancement of biosensors based on COF1 can be summarized in the following aspects: first, exposed carbonyl active sites of COF1 can promote the effective immobilization and bioactivity preserving of enzyme molecules; meanwhile, carbonyl groups also contribute to the enrichment of analyte TCh; second, the good conductivity of COF1 could facilitate electron transfer and response signal capturing of the electrochemical GC/COF1/AChE biosensor.

Determination of Paraoxon. We next used the GC/COF1/AChE biosensor to detect paraoxon, a model pesticide, because of its high toxicity and broad use in agriculture.[37,38] AChE will lose its ability to hydrolyze ATCh due to the blockage of the active site caused by the addition of paraoxon (Figure 5a). After exposure to paraoxon, the same GC/COF1/AChE electrode exhibited a significant drop in current, inspiring the quantification of paraoxon by the inhibition rate (Figure 5b). We next proceeded to optimize the inhibition time as it is important to enable adequate time for paraoxon to bind to the enzymes. As shown in Figure 5c, we found that

https://doi.org/10.1021/acssensors.2c02014
ACS Sens. XXXX, XXX, XXX−XXX

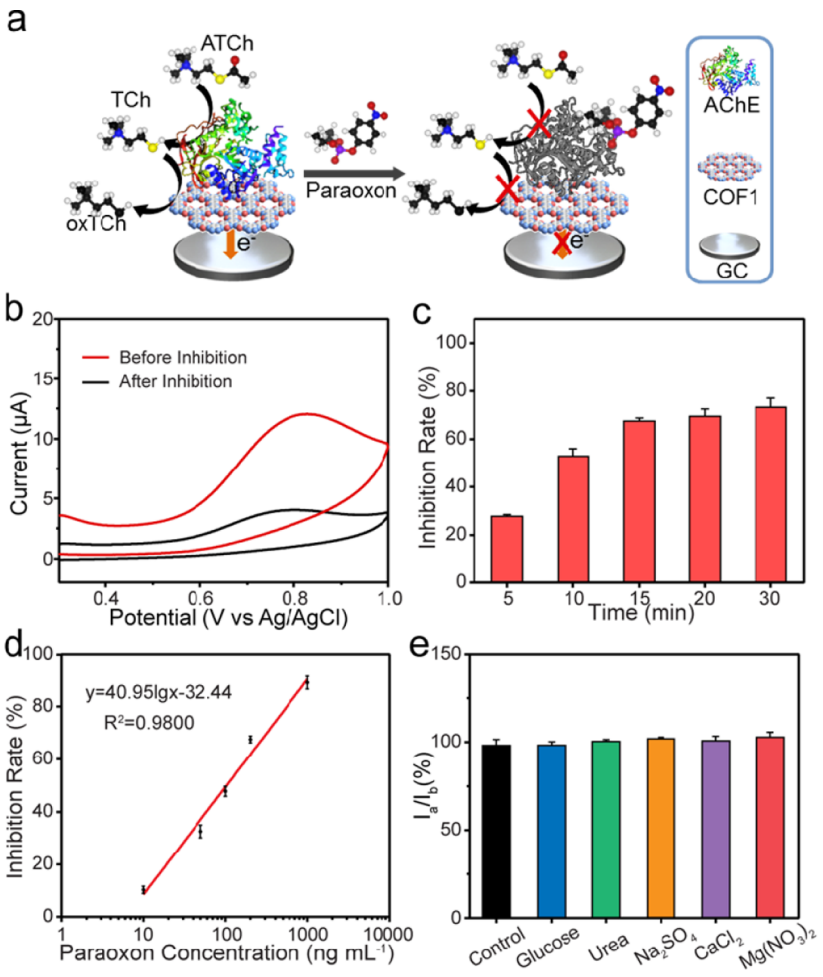

Figure 5. Determination of paraoxon. (a) Inhibition mechanism of GC/COF1/AChE electrodes by paraoxon. (b) CV of the GC/COF1/AChE electrode before and after incubation in 200 ng L^{-1} paraoxon. Scan rate: 100 mV s^{-1}. (c) Time-dependency of the inhibition rate increase. (d) Calibration plot showing the inhibition of the biosensor toward different concentrations of paraoxon, 10, 50, 100, 200 ng mL^{-1}, and 1 μg mL^{-1}. (e) Ratio of CV current of the biosensor after (I_a) and before (I_b) incubation in common interferents.

remarkable changes in the inhibition rate could be observed within 15 min. A further long inhibition time produced a stable inhibition rate, which means the saturation of the binding interaction between paraoxon and AChE. Therefore, 15 min was chosen in the next study because a shorter time was an important criterion for being an effective point-of-care analysis device. Inspired by these results, the GC/COF1/AChE electrode was employed to determine different concentrations of paraoxon. Figure 5d shows that there was a linear relationship between the inhibition rate and the concentration of paraoxon, ranging from 10 to 1000 ng mL^{-1}. The limit of detection (LOD) was determined to be 1.4 ng mL^{-1} through the equation LOD = 3σ/S (σ is the standard deviation of the current response in the paraoxon blank, and S is the slope of the standard curve). The LOD was significantly lower than the previous reports and the permissible maximum level (10 ppb) in the European Union pesticides database.[39−42] In addition, the sensitivity was determined to be nearly 41% per log concentration, much higher than that of biosensors modified with other nanomaterials, including Ag nanoparticle-modified MXene (9%),[43] AuPt hydrogels (19%),[44] and 2D fluoride-free Nb2CTx MXene (10%).[45] Thus, the GC/COF1/AChE biosensing system possessed a remarkable sensitivity and detection limit for paraoxon determination.

Selectivity, Practicability, and Stability of the Biosensor. Some potential interfering species were examined to assess the selectivity of the biosensor. As shown in Figure 5e, these compounds have been successfully verified to have no obvious effect on the electrochemical performance of the biosensor, which greatly demonstrated the reliability of the proposed paraoxon detection method. Tap water and cucumber were utilized as model samples in recovery experiments to further evaluate the practical use of the proposed biosensor. The recoveries of 100 ng mL^{-1} paraoxon obtained from tap water and cucumber were 102.9 and 117.6%, respectively, which were comparable to that of the LC−MS/MS method (Table S1), indicating the acceptable practicability of paraoxon monitoring from real samples. Besides, stability is also essential for the actual use of biosensors. In order to determine the stability of the biosensor, seven consecutive tests were taken. The rather steady biosensor responses were confirmed and are shown in Figure S10 by the relative standard deviation value of 1.9%. Furthermore, as shown in Figure S11, the biosensor retained 96.8% of the initial current response after 5 weeks of storage in a refrigerator at 4 °C, demonstrating the good long-term stability of the biosensor. The structural tunability and good conductivity of COFs make it attractive to investigate the

https://doi.org/10.1021/acssensors.2c02014
ACS Sens. XXXX, XXX, XXX−XXX

potential applications for signal amplification or monitoring of multiple contaminants.[46,47]

CONCLUSIONS

In summary, we synthesized 2D conductive COF1 with abundant carbonyl groups via a simple hydrothermal method. Its periodic aza-fused 2D π-conjugated structure could offer good chemical stability and high conductivity, inspiring us to investigate the possibility of using COF1 as electrode materials to prepare electrochemical enzymatic biosensors. The prepared COF1-based biosensor displayed a significantly enhanced electrochemical response compared to the biosensor without COF1. After a series of characterization and comparison experiments with the prepared COF2 without carbonyl groups, we proved the mechanism of signal enhancement. The exposed carbonyl active sites of COF1 can promote the effective immobilization and bioactivity preserving of enzyme molecules and contribute to the enrichment of TCh simultaneously. Besides, the good conductivity of COF1 also improved the biosensor performance. The research could pave the way for the significant potential applicability of 2D conductive COFs in electrochemical sensing applications. After optimizing experimental conditions, the biosensor demonstrated fast response speed, good selectivity and practicability, robust stability, and a low LOD of 1.4 ng mL^{-1} for paraoxon detection, which proves to be a promising method for the rapid and onsite detection of organophosphorus pesticides in the environment. We believe that our study paves the way for the enormous potential use of 2D conductive COFs as electrode materials in different sensing applications. Future work should focus on the development of novel conductive COF materials and new signal enhancement mechanisms to enable more sensitive electrochemical measurements.

ASSOCIATED CONTENT

Supporting Information

The Supporting Information is available free of charge at https://pubs.acs.org/doi/10.1021/acssensors.2c02014.

Apparatus and characterizations; solid-state ^{13}C NMR spectrum of COF1; Raman spectrum of COF1; high-resolution C1s, O 1s, and N 1s XPS spectra of COF1; synthesis route of COF2; FTIR spectra of HKH, TAB, and COF2; XRD patterns of COF2; FTIR spectra of COF2 and COF2-TCh; CVs of biosensors at different scan rates; CVs of COF1 and COF2 in $K_3Fe(CN)_6$/$K_4Fe(CN)_6$; stability and long-term stability of biosensors; and recovery test of paraoxon (PDF)

AUTHOR INFORMATION

Corresponding Author

Xianbo Lu − *CAS Key Laboratory of Separation Science for Analytical Chemistry, Dalian Institute of Chemical Physics, Chinese Academy of Sciences, Dalian, Liaoning 116023, P. R. China;* orcid.org/0000-0003-3983-7812; Email: xianbolu@dicp.ac.cn

Authors

Kai Niu − *CAS Key Laboratory of Separation Science for Analytical Chemistry, Dalian Institute of Chemical Physics, Chinese Academy of Sciences, Dalian, Liaoning 116023, P. R. China; University of Chinese Academy of Sciences, Beijing 100049, P. R. China*

Yuying Zhang − *CAS Key Laboratory of Separation Science for Analytical Chemistry, Dalian Institute of Chemical Physics, Chinese Academy of Sciences, Dalian, Liaoning 116023, P. R. China*

Jiping Chen − *CAS Key Laboratory of Separation Science for Analytical Chemistry, Dalian Institute of Chemical Physics, Chinese Academy of Sciences, Dalian, Liaoning 116023, P. R. China;* orcid.org/0000-0001-9404-1687

Complete contact information is available at: https://pubs.acs.org/10.1021/acssensors.2c02014

Author Contributions

X.L. designed research. K.N. performed research. Y.Z. performed the LC-MS/MS. K.N., J.C., and X.L. wrote the paper. All authors have given approval to the final version of the manuscript.

Notes

The authors declare no competing financial interest.

ACKNOWLEDGMENTS

This work was financially supported by the National Natural Science Foundation of China (grant nos. 22076181 and 22276185), the Dalian Science and Technology Innovation Fund (2020JJ26SN057), the Applied Basic Research Project of Liaoning Province (2022JH2/101300098), and the DICP (grant no. DICP I202001).

REFERENCES

(1) Côté, A. P.; Benin, A. I.; Ockwig, N. W.; O'Keeffe, M.; Matzger, A. J.; Yaghi, O. M. Porous, crystalline, covalent organic frameworks. *Science* **2005**, *310*, 1166.

(2) Zhang, W. W.; Chen, L. J.; Dai, S.; Zhao, C. X.; Ma, C.; Wei, L.; Zhu, M. H.; Chong, S. Y.; Yang, H. F.; Liu, L. J.; Bai, Y.; Yu, M. J.; Xu, Y. J.; Zhu, X. W.; Zhu, Q.; An, S. H.; Sprick, R. S.; Little, M. A.; Wu, X. F.; Jiang, S.; Wu, Y. Z.; Zhang, Y. B.; Tian, H.; Zhu, W. H.; Cooper, A. I. Reconstructed covalent organic frameworks. *Nature* **2022**, *604*, 72−79.

(3) Sun, T.; Xie, J.; Guo, W.; Li, D. S.; Zhang, Q. C. Covalent-Organic Frameworks: Advanced Organic Electrode Materials for Rechargeable Batteries. *Adv. Energy Mater.* **2020**, *10*, 1904199.

(4) Wang, D. G.; Qiu, T. J.; Guo, W. H.; Liang, Z. B.; Tabassum, H.; Xia, D. G.; Zou, R. Q. Covalent organic framework-based materials for energy applications. *Energy Environ. Sci.* **2021**, *14*, 688−728.

(5) Jin, F. Z.; Lin, E.; Wang, T. H.; Geng, S. B.; Wang, T.; Liu, W. S.; Xiong, F. H.; Wang, Z. F.; Chen, Y.; Cheng, P.; Zhang, Z. J. Bottom-Up Synthesis of 8-Connected Three-Dimensional Covalent Organic Frameworks for Highly Efficient Ethylene/Ethane Separation. *J. Am. Chem. Soc.* **2022**, *144*, 5643−5652.

(6) Yu, C. Y.; Li, H.; Wang, Y. J.; Suo, J. Q.; Guan, X. Y.; Wang, R.; Valtchev, V.; Yan, Y. S.; Qiu, S. L.; Fang, Q. R. Three-Dimensional Triptycene-Functionalized Covalent Organic Frameworks with hea Net for Hydrogen Adsorption. *Angew. Chem. Int. Edit.* **2022**, *61*, No. e202117101.

(7) Wang, M. C.; Ballabio, M.; Wang, M.; Lin, H. H.; Biswal, B. P.; Han, X. C.; Paasch, S.; Brunner, E.; Liu, P.; Chen, M. W.; Bonn, M.; Heine, T.; Zhou, S. Q.; Cánovas, E.; Dong, R. H.; Feng, X. L. Unveiling Electronic Properties in Metal-Phthalocyanine-Based Pyrazine-Linked Conjugated Two-Dimensional Covalent Organic Frameworks. *J. Am. Chem. Soc.* **2019**, *141*, 16810−16816.

(8) Banerjee, T.; Podjaski, F.; Kröger, J.; Biswal, B. P.; Lotsch, B. V. Polymer photocatalysts for solar-to-chemical energy conversion. *Nat. Rev. Mater.* **2021**, *6*, 168−190.

(9) Han, B.; Ding, X.; Yu, B. Q.; Wu, H.; Zhou, W.; Liu, W. P.; Wei, C. Y.; Chen, B. T.; Qi, D. D.; Wang, H. L.; Wang, K.; Chen, Y. L.; Chen, B. L.; Jiang, J. Z. Two-Dimensional Covalent Organic

Frameworks with Cobalt(II)-Phthalocyanine Sites for Efficient Electrocatalytic Carbon Dioxide Reduction. *J. Am. Chem. Soc.* **2021**, *143*, 7104−7113.
(10) Li, F.; Kan, J. L.; Yao, B. J.; Dong, Y. B. Synthesis of Chiral Covalent Organic Frameworks via Asymmetric Organocatalysis for Heterogeneous Asymmetric Catalysis. *Angew. Chem. Int. Edit.* **2022**, *61*, No. e202115044.
(11) Zhang, G. Y.; Li, X. L.; Liao, Q. B.; Liu, Y. F.; Xi, K.; Huang, W. Y.; Jia, X. D. Water-dispersible PEG-curcumin/amine-functionalized covalent organic framework nanocomposites as smart carriers for in vivo drug delivery. *Nat. Commun.* **2018**, *9*, 2785.
(12) Ge, L.; Qiao, C. Y.; Tang, Y. K.; Zhang, X. K.; Jiang, X. Q. Light-Activated Hypoxia-Sensitive Covalent Organic Framework for Tandem-Responsive Drug Delivery. *Nano Lett.* **2021**, *21*, 3218−3224.
(13) Peng, Y. W.; Huang, Y.; Zhu, Y. H.; Chen, B.; Wang, L. Y.; Lai, Z. C.; Zhang, Z. C.; Zhao, M. T.; Tan, C. L.; Yang, N. L.; Shao, F. W.; Han, Y.; Zhang, H. Ultrathin Two-Dimensional Covalent Organic Framework Nanosheets: Preparation and Application in Highly Sensitive and Selective DNA Detection. *J. Am. Chem. Soc.* **2017**, *139*, 8698−8704.
(14) Kaczmarek, A. M.; Liu, Y. Y.; Kaczmarek, M. K.; Liu, H. S.; Artizzu, F.; Carlos, L. D.; Van Der Voort, P. Developing Luminescent Ratiometric Thermometers Based on a Covalent Organic Framework (COF). *Angew. Chem. Int. Edit.* **2020**, *59*, 1932−1940.
(15) Mishra, R. K.; Goud, K. Y.; Li, Z. H.; Moonla, C.; Mohamed, M. A.; Tehrani, F.; Teymourian, H.; Wang, J. Continuous Opioid Monitoring along with Nerve Agents on a Wearable Microneedle Sensor Array. *J. Am. Chem. Soc.* **2020**, *142*, 5991−5995.
(16) Zhou, Z. Y.; Mukherjee, S.; Hou, S. J.; Li, W. J.; Elsner, M.; Fischer, R. A. Porphyrinic MOF Film for Multifaceted Electrochemical Sensing. *Angew. Chem. Int. Edit.* **2021**, *60*, 20551−20557.
(17) Yu, P.; Wei, H.; Zhong, P. P.; Xue, Y. F.; Wu, F.; Liu, Y.; Fei, J. J.; Mao, L. Q. Single-Carbon-Fiber-Powered Microsensor for In Vivo Neurochemical Sensing with High Neuronal Compatibility. *Angew. Chem. Int. Edit.* **2020**, *59*, 22652−22658.
(18) Jin, J.; Ji, W. L.; Li, L. J.; Zhao, G.; Wu, W. J.; Wei, H.; Ma, F. R.; Jiang, Y.; Mao, L. Q. Electrochemically Probing Dynamics of Ascorbate during Cytotoxic Edema in Living Rat Brain. *J. Am. Chem. Soc.* **2020**, *142*, 19012−19016.
(19) Li, W. K.; Ren, P.; Zhou, Y. W.; Feng, J. T.; Ma, Z. Q. Europium(III) functionalized 3D covalent organic framework for quinones adsorption and sensing investigation. *J. Hazard. Mater.* **2020**, *388*, 121740.
(20) Wang, J. M.; Qu, X. L.; Zhao, L. M.; Yan, B. Fabricating Nanosheets and Ratiometric Detection of 5-Fluorouracil by Covalent Organic Framework Hybrid Material. *Anal. Chem.* **2021**, *93*, 4308−4316.
(21) Liang, H.; Xu, H. B.; Zhao, Y. T.; Zheng, J.; Zhao, H.; Li, G. L.; Li, C. P. Ultrasensitive electrochemical sensor for prostate specific antigen detection with a phosphorene platform and magnetic covalent organic framework signal amplifier. *Biosens. Bioelectron.* **2019**, *144*, 111691.
(22) Feng, S. N.; Yan, M. X.; Xue, Y.; Huang, J. S.; Yang, X. R. Electrochemical Immunosensor for Cardiac Troponin I Detection Based on Covalent Organic Framework and Enzyme-Catalyzed Signal Amplification. *Anal. Chem.* **2021**, *93*, 13572−13579.
(23) Liu, X.; Huang, D.; Lai, C.; Zeng, G.; Qin, L.; Wang, H.; Yi, H.; Li, B.; Liu, S.; Zhang, M.; Deng, R.; Fu, Y.; Li, L.; Xue, W.; Chen, S. Recent advances in covalent organic frameworks (COFs) as a smart sensing material. *Chem. Soc. Rev.* **2019**, *48*, 5266−5302.
(24) Yang, H.; Li, F. S.; Zhan, S. Q.; Liu, Y. W.; Li, W. L.; Meng, Q. J.; Kravchenko, A.; Liu, T. Q.; Yang, Y.; Fang, Y.; Wang, L. Q.; Guan, J. Q.; Furó, I.; Ahlquist, M. S. G.; Sun, L. C. Intramolecular hydroxyl nucleophilic attack pathway by a polymeric water oxidation catalyst with single cobalt sites. *Nat. Catal.* **2022**, *5*, 414−429.
(25) Meng, Z.; Aykanat, A.; Mirica, K. A. Proton Conduction in 2D Aza-Fused Covalent Organic Frameworks. *Chem. Mater.* **2019**, *31*, 819−825.
(26) Li, X. L.; Wang, H. X.; Chen, H.; Zheng, Q.; Zhang, Q. B.; Mao, H. Y.; Liu, Y. W.; Cai, S. L.; Sun, B.; Dun, C. C.; Gordon, M. P.; Zheng, H. M.; Reimer, J. A.; Urban, J. J.; Ciston, J.; Tan, T. W.; Chan, E. M.; Zhang, J.; Liu, Y. Dynamic Covalent Synthesis of Crystalline Porous Graphitic Frameworks. *Chem* **2020**, *6*, 933−944.
(27) Sidhu, G. K.; Singh, S.; Kumar, V.; Dhanjal, D. S.; Datta, S.; Singh, J. Toxicity, monitoring and biodegradation of organophosphate pesticides: A review. *Crit. Rev. Environ. Sci. Technol.* **2019**, *49*, 1135−1187.
(28) Aroniadou-Anderjaska, V.; Apland, J. P.; Figueiredo, T. H.; De Araujo Furtado, M. D.; Braga, M. F. Acetylcholinesterase inhibitors (nerve agents) as weapons of mass destruction: History, mechanisms of action, and medical countermeasures. *Neuropharmacology* **2020**, *181*, 108298.
(29) Kandambeth, S.; Jia, J. T.; Wu, H.; Kale, V. S.; Parvatkar, P. T.; Czaban-Jóźwiak, J.; Zhou, S.; Xu, X. M.; Ameur, Z. O.; Abou-Hamad, E.; Emwas, A. H.; Shekhah, O.; Alshareef, H. N.; Eddaoudi, M. Covalent Organic Frameworks as Negative Electrodes for High-Performance Asymmetric Supercapacitors. *Adv. Energy Mater.* **2020**, *10*, 2001673.
(30) Tian, Z. N.; Kale, V. S.; Wang, Y. Z.; Kandambeth, S.; Czaban-Jóźwiak, J.; Shekhah, O.; Eddaoudi, M.; Alshareef, H. N. High-Capacity NH4+ Charge Storage in Covalent Organic Frameworks. *J. Am. Chem. Soc.* **2021**, *143*, 19178−19186.
(31) Fan, G. H.; Li, X.; Liu, J. Y.; He, G. Z. Excited-state properties of a blue luminescent covalent organic framework by the time-dependent density-functional tight-binding method. *Comput. Theor. Chem.* **2014**, *1030*, 17−24.
(32) Aiyappa, H. B.; Thote, J.; Shinde, D. B.; Banerjee, R.; Kurungot, S. Cobalt-Modified Covalent Organic Framework as a Robust Water Oxidation Electrocatalyst. *Chem. Mater.* **2016**, *28*, 4375−4379.
(33) Wu, M. M.; Zhao, Y.; Sun, B. Q.; Sun, Z. H.; Li, C. X.; Han, Y.; Xu, L. Q.; Ge, Z.; Ren, Y. X.; Zhang, M. T.; Zhang, Q.; Lu, Y.; Wang, W.; Ma, Y. F.; Chen, Y. S. A 2D covalent organic framework as a high-performance cathode material for lithium-ion batteries. *Nano Energy* **2020**, *70*, 104498.
(34) Lei, Y.; Butler, D.; Lucking, M. C.; Zhang, F.; Xia, T. N.; Fujisawa, K.; Granzier-Nakajima, T.; Cruz-Silva, R.; Endo, M.; Terrones, H.; Terrones, M.; Ebrahimi, A. Single-atom doping of MoS2 with manganese enables ultrasensitive detection of dopamine: Experimental and computational approach. *Sci. Adv.* **2020**, *6*, No. eabc4250.
(35) Wu, Y.; Jiao, L.; Luo, X.; Xu, W. Q.; Wei, X. Q.; Wang, H. J.; Yan, H. Y.; Gu, W. L.; Xu, B. Z.; Du, D.; Lin, Y. H.; Zhu, C. Z. Oxidase-Like Fe-N-C Single-Atom Nanozymes for the Detection of Acetylcholinesterase Activity. *Small* **2019**, *15*, 1903108.
(36) Du, X.; Zhang, Z. H.; Zheng, X. D.; Zhang, H. Y.; Dong, D.; Zhang, Z. G.; Liu, M.; Zhou, J. An electrochemical biosensor for the detection of epithelial-mesenchymal transition. *Nat. Commun.* **2020**, *11*, 192.
(37) Chen, Y. J.; Zhang, Z.; Zhuang, J.; Lee, J. H.; Wang, L. C.; Fang, R. H.; Gao, W. W.; Zhang, L. F. Cell-Membrane-Cloaked Oil Nanosponges Enable Dual-Modal Detoxification. *ACS Nano* **2019**, *13*, 7209−7215.
(38) Zhang, L. B.; Baker, S. L.; Murata, H.; Harris, N.; Ji, W. H.; Amitai, G.; Matyjaszewski, K.; Russell, A. J. Tuning Butyrylcholinesterase Inactivation and Reactivation by Polymer-Based Protein Engineering. *Adv. Sci.* **2020**, *7*, 1901904.
(39) Sgobbi, L. F.; Machado, S. A. S. Functionalized polyacrylamide as an acetylcholinesterase-inspired biomimetic device for electrochemical sensing of organophosphorus pesticides. *Biosens. Bioelectron.* **2018**, *100*, 290−297.
(40) Robidillo, C. J. T.; Wandelt, S.; Dalangin, R.; Zhang, L.; Yu, H.; Meldrum, A.; Campbell, R. E.; Veinot, J. G. C. Ratiometric Detection of Nerve Agents by Coupling Complementary Properties of Silicon-Based Quantum Dots and Green Fluorescent Protein. *ACS Appl. Mater. Inter.* **2019**, *11*, 33478−33488.
(41) Tang, W.; Yang, J.; Wang, F.; Wang, J.; Li, Z. Thiocholine-triggered reaction in personal glucose meters for portable quantitative

https://doi.org/10.1021/acssensors.2c02014
ACS Sens. XXXX, XXX, XXX−XXX

detection of organophosphorus pesticide. *Anal. Chim. Acta* **2019**, *1060*, 97−102.
(42) Bordbar, M. M.; Nguyen, T. A.; Arduini, F.; Bagheri, H. A paper-based colorimetric sensor array for discrimination and simultaneous determination of organophosphate and carbamate pesticides in tap water, apple juice, and rice. *Mikrochim. Acta* **2020**, *187*, 621.
(43) Jiang, Y. J.; Zhang, X. N.; Pei, L. J.; Yue, S.; Ma, L.; Zhou, L. Y.; Huang, Z. H.; He, Y.; Gao, J. Silver nanoparticles modified two-dimensional transition metal carbides as nanocarriers to fabricate acetycholinesterase-based electrochemical biosensor. *Chem. Eng. J.* **2018**, *339*, 547−556.
(44) Wu, Y.; Jiao, L.; Xu, W.; Gu, W.; Zhu, C.; Du, D.; Lin, Y. Polydopamine-Capped Bimetallic AuPt Hydrogels Enable Robust Biosensor for Organophosphorus Pesticide Detection. *Small* **2019**, *15*, No. e1900632.
(45) Song, M.; Pang, S. Y.; Guo, F.; Wong, M. C.; Hao, J. Fluoride-Free 2D Niobium Carbide MXenes as Stable and Biocompatible Nanoplatforms for Electrochemical Biosensors with Ultrahigh Sensitivity. *Adv. Sci.* **2020**, *7*, 2001546.
(46) Liu, J. C.; Xing, Y. P.; Xue, B. Y.; Zhou, X. H. Nanozyme enhanced paper-based biochip with a smartphone readout system for rapid detection of cyanotoxins in water. *Biosens. Bioelectron.* **2022**, *205*, 114099.
(47) Zhu, Q.; Liu, L. H.; Wang, R. Y.; Zhou, X. H. A split aptamer (SPA)-based sandwich-type biosensor for facile and rapid detection of streptomycin. *J. Hazard. Mater.* **2021**, *403*, 123941.

https://doi.org/10.1021/acssensors.2c02014
ACS Sens. XXXX, XXX, XXX−XXX